Kapβ2 is a modifier of the C9orf72-linked glycine-arginine dipeptide neurotoxicity

Cicardi ME[1], Kankate V[1], Sriramoji S[1], Krishnamurthy K[1], Markandaiah SS[1], Verdone BM[1], Girdhar A[2], Nelson A[1], Rivas LB[1], Boehringer A[1], Haeusler AR[1], Pasinelli P[1], Guo L[2], Trotti D[1].

[1]Jefferson Weinberg ALS Center, Vickie and Jack Farber Institute for Neuroscience, Department of Neuroscience, Thomas Jefferson University, Philadelphia, PA, USA

[2]Department of Biochemistry and Molecular Biology, Thomas Jefferson University, Philadelphia, PA, USA

Correspondence:
Davide Trotti, Ph.D.
Jefferson Hospital for Neuroscience building, 4th floor, room 416
900 Walnut Street, Philadelphia, PA 19107, USA
Tel. 215-955-8416
Email davide.trotti@jefferson.edu

Summary

A common cause of amyotrophic lateral sclerosis and frontotemporal dementia is the presence of a G_4C_2 intronic expansion in the *C9orf72* gene. This expansion is translated by a non-AUG-dependent mechanism into five different dipeptide repeat proteins (DPRs), including the aggregation-prone poly glycine-arginine (GR), which is neurotoxic. Poly(GR) was found to interact with the nuclear importin Kapβ2 in non-neuronal cell lines. However, whether this interaction also occurs in neurons impacting their survival has not been studied. Here, we demonstrated that Kapβ2 and poly(GR) co-aggregate in neurons *in-vitro* and *in-vivo* in CNS tissue. Moreover, we showed that Kapβ2 mitigates poly(GR) neurotoxicity. Indeed, overexpression of Kapβ2 relieved poly(GR)-mediated neurotoxicity and restored nuclear TDP-43 levels, whereas silencing Kapβ2 increased the risk of death of neurons expressing poly(GR), suggesting that Kapβ2 plays a critical role in neurodegeneration. These findings open a new therapeutic avenue in C9-linked ALS/FTD focused on modulating Kapβ2 levels.

Keywords

C9orf72, ALS, FTD, karyopherin β2, dipeptide repeat proteins, TNPO1, TDP-43

INTRODUCTION

The most common genetic cause of amyotrophic lateral sclerosis (ALS), a fatal neurodegenerative disease (Feldman et al., 2022), is a non-coding G_4C_2 nucleotide repeat expansion (NRE) in the *C9orf72* gene (DeJesus-Hernandez et al., 2011, Renton et al., 2011). This NRE can be aberrantly translated through a process known as repeat-associated non-AUG translation (RAN-T), leading to the production of five different dipeptide repeat proteins (DPRs): poly(GA), poly(GP), poly (GR), poly(PA), and poly(PR) (Gendron and Petrucelli, 2017). Arginine-rich (R-rich) DPRs are neurotoxic, possibly in a length-dependent manner (Wen et al., 2014a, Verdone et al., 2022). *In-vitro* models have been employed to identify dysregulated pathways caused by the accumulation of poly(GR) and poly(PR), such as translation stalling, stress granules persistence, nucleolar stress, DNA damage, and nuclear pore complex defects (Coyne et al., 2020, Moens et al., 2019, Maor-nof et al., 2020, Chew et al., 2019b). Long poly(GR) dipeptides (≥200) cause TDP-43 translocation from the nucleus to the cytoplasm. This process is a well-known pathological hallmark of ALS (Cook et al., 2020), while poly$(GR)_{80}$ expressing mice have behavioral impairments but lack TDP-43 mislocalization (Choi 2019). We recently established a mouse model constitutively expressing an intermediate GR length, poly$(GR)_{50}$, which develops mild behavioral and synaptic phenotypes (Verdone et al., 2022). While this model did not display TDP-43 mislocalization, it did show defects in the nuclear pore complex integrity, as revealed in aged mice by Nup62 mislocalization in the cytoplasm (Gleixner et al., 2022), suggesting that nuclear pore complex integrity does not univocally associate with neurodegeneration.

The poly(GR) interactome is composed of many proteins, most of which feature low complexity domains, through which the interaction with poly(GR) occurs, including RNA-binding proteins, nucleolar components, stress granules components, and proteins involved in nuclear transport (Lee et al., 2016). Among the latter is karyopherin β2 (Kapβ2, also known as transportin-1 or Importin β2), which belongs to the family of nuclear import receptors (NIRs) that orchestrate the exchange of proteins between the nucleus and cytoplasm (Stewart, 2007). Even though no ALS-causative mutations in the *KAPβ2* gene have been identified thus far, the KAPβ2 protein interacts with many ALS-causative proteins such as FUS, but also TAF, EWS, hnRNPA1,

and hnRNPA2 (Neumann et al., 2012, Takeuchi et al., 2013, Troakes et al., 2013, Guo et al., 2019). Interestingly, the domain of these proteins involved in the interaction with Kapβ2 is a PY-NLS, a non-common nuclear localization signal rich in prolines (P) and tyrosines (Y), in which many of the most common and aggressive ALS-related mutations are found (Twyffels et al., 2014, Gonzalez et al., 2021, Xue et al., 2020). Poly(GR), even at very short lengths (e.g., 10 repeats), is predicted to interact with Kapβ2 *via* the same domain in Kapβ2 (Hayes et al., 2020). Notably, poly(GR) is known to affect the localization of proteins in the nucleus (Hutten et al., 2020). But it is still unclear whether it does it by interacting directly with the proteins of interest or with the NIR responsible for their nuclear localization. Moreover, and most notably, all the studies published thus far aimed at examining poly(GR)-Kapβ2 interactions have been carried out in non-neuronal cells, raising questions about their ALS disease relevance.

In this work, we report that poly(GR) interacts with Kapβ2 in primary neurons and CNS tissues of a poly(GR) mouse model, supporting the disease relevance of this interaction. We then explore the relevance of this interaction for neuronal survival. We observe that reduced levels of Kapβ2 are detrimental to neuronal survivability in the presence of poly(GR). On the contrary, increased Kapβ2 greatly mitigates poly(GR) toxicity. We also show that Kapβ2 can counteract poly(GR) neurotoxicity by restoring nuclear TDP-43 localization. These results prove that Kapβ2 is a positive modifier of the disease. Manipulations of its expression might be harnessed to design future therapy strategies.

RESULTS

Poly(GR) interacts with Kapβ2 in neurons

Kapβ2 was previously shown to interact with poly(GR) in non-neuronal cell line models (Hutten et al., 2020, Hayes et al., 2020). To determine whether this interaction could also occur in disease-relevant cells, we ectopically expressed poly(GR)$_{50}$ in primary cortical neurons by transducing a lentivirus expression vector encoding the arginine-rich dipeptide repeat protein GR$_{50}$ (Flag and GFP tagged at the N- and C-terminus, respectively), and driven by the neuronal-specific human

synapsin promoter (hSyn). Immunofluorescence staining of the transduced neurons revealed that Kapβ2 displayed perinuclear and cytoplasmic localization (**Fig. 1A**). To assess whether GR_{50} and Kapβ2 co-localize in the same cellular compartments, we measured in transduced neurons the Pearson's correlation coefficient to estimate the extent of co-localization between Kapβ2 and GR_{50}. GFP was used as a control for this assessment. We determined that the co-localization coefficient was significantly higher in GR_{50}-expressing neurons compared to the ones transduced with GFP (Flag-GFP) alone (**Fig. 1B**).

To further evaluate whether, in addition to co-localizing, these two proteins also interact, we performed co-immunoprecipitation (co-IP), taking advantage of the Flag reporter tag fused with the encoded proteins. GFP immunopositive bands running on an SDS-PAGE gel at the expected molecular weights of GFP and GR_{50}-GFP were detected in the input and the Co-IP lanes of the Western blot (**Fig 1C-S1B**). However, Kapβ2 co-precipitated with GR_{50}-GFP but not with GFP alone, suggesting that the interaction is determined by GR_{50} and not by the GFP reporter moiety (**Fig. 1C**).

To determine whether the Kapβ2-poly(GR) interaction would also occur in an *in-vivo* setting, we used a recently developed transgenic mouse that expresses GR_{50}-GFP prevalently in neurons throughout the CNS, recently developed in our laboratory, in which the expression of either Flag-GFP or Flag-GR_{50}-GFP is elicited by *Cre*-recombinase (Verdone et al., 2022). Immunoprecipitations were performed on the whole brain and spinal cord lysates of 12-month-old mice that were generated by crossing Flag-GFP or Flag-GR_{50}-GFP mice with a ubiquitously expressing *Cre* mouse line. Similar to what we found *in-vitro* in neurons, Kapβ2 co-immunoprecipitated with GR_{50}-GFP but not with GFP or IgG control groups (**Fig. 1D-S2C-D**).

Moreover, Kapβ2 immunofluorescence staining was performed in GR_{50}-GFP cerebral cortex and spinal cord sections. In wild-type CNS tissues, the perinuclear and cytoplasmic staining patterns of Kapβ2 reminisced of the pattern we observed in primary cortical neurons (**Suppl. Fig. 3A**). We performed a 3D rendering to visualize better Kapβ2 localization inside both forebrain and spinal cord neurons (Imaris software). A strong co-localization of Kapβ2 and GR_{50}-GFP (Pearson's coefficient between 0.5 and 1 in both tissues) was identified in NeuN-positive cells (**Fig. 1E-F, Suppl. Video 1**). Using a whole tissue immunostaining protocol followed by tissue

clearing we probed for Kapβ2 in a GR_{50} mouse brain and we acquired images with a light sheet microscope. We again observed the presence GR/Kapβ2 immunopositive areas inside *bonafide,* $NeuN^+$, neuronal cells.

Poly(GR) aggregates are also found in postmortem tissues of C9-ALS/FTD patients, and their abundance varies in different brain regions (Schludi et al., 2015). Kapβ2 expression levels in disease, however, did not change as determined by Western blot analysis performed on spinal cord sample lysates from C9-ALS/FTD cases and non-diseased control cases (**Fig. 1G-H**), suggesting that the poly(GR) pathology is not dependent on the Kapβ2 expression levels.

Kapβ2 prevents poly(GR) neurotoxicity

After evaluating the interaction of Kap2 with poly(GR), we sought to determine whether this interaction could play a role in modifying the neurotoxic properties of poly(GR). We thus knocked down Kapβ2 expression in neurons and then assessed the viability of poly(GR) expressing neurons.

We used a pool of four siRNAs designed against Kapβ2 RNA transcripts to achieve significant Kapβ2 reduction in neurons. Forty-eight hours after transfection, RNA and protein levels significantly decreased by 21.7±7.6% and 64.6±23.1%, respectively (Fig. 2 A-C). In Kapβ2 silenced neurons, we expressed poly(GR) and assessed the viability of these neurons. The risk of death increased significantly on day 7 in the Kapβ2 silenced, poly(GR)-expressing neurons compared to those treated with Kapβ2 scramble siRNA (**Fig. 2 D-E**), suggesting that the expression levels of Kapβ2 affect poly(GR) toxicity. We, therefore, hypothesized that increasing the levels of Kapβ2 might play a beneficial role and expressed GFP-Kapβ2 in primary cortical neurons to test this hypothesis. Transduced GFP-Kapβ2 localized in cytoplasmic puncta that mainly surround the nucleus, as expected (**Fig. 3A, Movie 2**). To first ensure that the heterologous Kapβ2 expression did not cause intrinsic toxicity, we imaged neurons that were transfected with expression vectors encoding the cell filling hSyn-Td-Tomato (Tom^+) construct and GFP-Kapβ2 or GFP alone at two different DNA concentrations (400 and 800 ng/well). We then assessed the survival of transfected neurons over several days in culture. Over 14 days, the cumulative survival curve of GFP-Kapβ2 transfected neurons was not different from that of GFP-expressing neurons at both tested

concentrations (**Fig. 3B-E** and **Table 1**), indicating that increasing Kapβ2 expression in neurons is not detrimental to their viability *in-vitro* overtime. Expression of poly(GR) of different repeat lengths (50, 100, and 200) in primary cortical neurons increased their risk of death in a length-dependent manner (Wen et al., 2014b, Verdone et al., 2022). Thus we co-transfected GFP- and either Flag-GR_{50}-mCherry, FLAG-GR_{100}-mCherry, or Flag-mCherry in neurons and observed the recruitment of Kapβ2 by poly(GR) is dependent on its repeat length. This was quantified by measuring the Pearson's coefficient for colocalization of GFP-Kapβ2 with GR_{50}-mCherry and GR_{100}-mCherry (**Fig. 4A-B**). We also plotted fluorescent intensity profiles for GR_{50}-mCherry and GR_{100}-mCherry cytoplasmic aggregates. This analysis showed an overlap between the intensity profile of both GR_{50}-mCherry and GR_{100}-mCherry aggregates and GFP-Kapβ2 (**Fig. 4C, D**). Neuronal viability was determined by performing time-lapse, live-cell imaging, and Kaplan-Meier analysis of survival of groups of neurons transfected with a 1:1 ratio of GFP-Kapβ2 (or GFP alone) and poly(GR)-mCherry (or mCherry alone).

GFP/mCherry-positive neurons were imaged for 8 days, and Kaplan-Meier survival curves were built (**Fig 4 E-F, Table 1**). GR_{50}-mCherry and GR_{100}-mCherry caused decreased neuronal viability compared to controls (mCherry vs. GR_{50}-mCherry $p< 0.0001$; mCherry vs. GR_{100}-mCherry $p< 0.0001$) as previously reported (Wen et al., 2014b, Verdone et al., 2022). Interestingly, expression of GFP-Kapβ2 in GR_{50}-mCherry neurons increased their survival to levels comparable to mCherry-expressing control neurons (GR_{50}-mCherry vs. GR_{50}-mCherry/Kapβ2 $p<0.0001$; GR_{100}-mCherry vs. GR_{100}-mCherry/Kapβ2 $p=0.005$) (**Table 2**) indicating that Kapβ2 rescues neurons from poly(GR) time-dependent toxicity.

Kapβ2 does not affect the dynamic properties of the poly(GR) aggregates.

The interaction of Kapβ2 with FUS aggregates can alter the dynamic properties of the aggregates themselves. Indeed, Kapβ2 overexpression can delay phase separation of FUS and the formation of insoluble gel-like structures of mutant FUS (Guo et al., 2018). We hypothesized that a similar effect could also occur in the case of poly(GR) aggregates. We, therefore, determined whether the heterologous expression of Kapβ2 would ultimately alter the physical properties of the poly(GR) aggregates. GFP-Kapβ2 and poly(GR)-mCherry were expressed in HEK-293 cells, and

FRAP (Fluorescence Recovery after Photobleaching) was staged on aggregates that were green and red fluorescent, therefore positive for both poly(GR)-mCherry and GFP-Kapβ2 (**Fig. 5A-F**). After having photobleached GR_{50}-mCherry or GR_{100}-mCherry aggregates, the fluorescence intensity of this region of interest was measured for 3 minutes. The percentage of mCherry recovery over this time frame was not affected by the presence of GFP-Kapβ2 (**Fig. 5 A, C, E**). These results align with a previous report that showed that Kapβ2 interaction with poly(GR) did not change the molecular interactions inside the aggregates (Hutten et al., 2020a).

Kapβ2 restores nuclear TDP-43 in poly(GR)-expressing neurons.

Expression of poly(GR) in neurons leads to the re-localization of TDP-43 from the nucleus to the cytoplasm (Zhang et al., 2015). Poly(GR) was also shown to form co-aggregates with TDP-43. It has been demonstrated that Kapβ2 prevents poly(GR) from interacting with other proteins, which might be trapped in poly(GR) aggregates. Kapβ2 would act as a shield that, by preventing poly(GR) aberrant interaction, allows other potentially interacting proteins to partition within the cell correctly.

Therefore, we examined TDP-43 localization in poly(GR)$^+$ neurons after we expressed Kapβ2. TDP-43 nuclear intensity in cells positive for both GFP-Kapβ2 and GR_{50}-mCherry was significantly higher than in cells positive for both GFP and GR_{50}-mCherry (**Fig. 6 A, B**) ($p<0.05$). A similar pattern was observed for GR_{100}-mCherry (**Fig. 6 A, B**). Indeed, in cells expressing both GFP-Kapβ2 and GR_{100}-mCherry, TDP-43 nuclear staining showed higher intensity than in cells that were positive for GFP as control and GR_{100}-mCherry.

We further assessed whether TDP-43 nuclear re-localization was attributed to a diminished interaction with poly(GR) consequential to Kapβ2. To test this hypothesis, we performed an *in vitro* experiment in which GR/TDP-43 aggregates were allowed to form in the presence and absence of Kapβ2. We used an equimolar concentration of 5 μM for all three proteins. Poly (GR) and TDP-43, when combined *in vitro,* form large condensates (**Fig. 6C**), which remain mostly soluble in the presence of Kapβ2. Interestingly, the addition of Kapβ2 did not only reduce aggregates size but also increased the diffusive TDP-43 fluorescence signal outside the aggregates (**Fig. 6 C, D**), suggesting that the interaction between Kapβ2 and poly(GR) functions

as a shield against the interaction of poly(GR) with other proteins like TDP-43 (Hutten et al., 2020).

DISCUSSION

In this study, we established the role of Kapβ2 in modulating poly(GR) neuronal toxicity. We first observed that poly(GR) interacts with Kapβ2 in neurons both *in-vitro* and *in-vivo*. We then reported that silencing Kapβ2 increases the risk of death of neurons expressing poly(GR). Interestingly, overexpression of Kapβ2 protects neurons from neurodegeneration induced by poly(GR). Finally, we evaluated the molecular mechanisms associated with Kapβ2 mediated mitigation of poly(GR) toxicity. In line with previous evidence (Hutten et al., 2020), we showed that Kapβ2 did not change the dynamic properties of poly(GR) aggregates. It did, however, increase the nuclear localization of TDP-43. TDP-43 mislocalization is a hallmark of toxicity in ALS, and TDP-43 pathology is found in ~97% of ALS patients, including C9-ALS patients. It has already been demonstrated that poly(GR) causes TDP-43 mislocalization from the nucleus to the cytoplasm (Cook et al., 2020). The mislocalization of TDP-43 in the presence of poly(GR) protein is not caused by loss of nuclear integrity but instead by poly(GR) interference with the nuclear transport (Hutten et al., 2020). Even more interestingly, two different studies show that poly(GR) can obstruct both canonical, importin α, and β mediated (Hayes et al., 2020) and non-canonical nuclear import (Hutten et al., 2020). In light of these previous studies and our results, we propose a mechanism by which Kapβ2 counteracts poly(GR) toxicity by interacting with poly(GR) and acting as a shield. Indeed, preventing poly(GR) from interacting with TDP-43 leaves TDP-43 free to re-enter the nucleus. In forming the shield to free crucial proteins like TDP-43, the stoichiometry of the binding between KapB2 and poly(GR) is crucial. Indeed, these results suggest a model in which the relative amount of poly(GR) and Kapβ2 play a critical role. There is a homeostatic status in which the Kapβ2/poly(GR) ratio is either in favor of Kapβ2 or at equilibrium (Kapβ2 $\geq$ poly(GR)). When Kapβ2/poly(GR) ratio is instead in favor of poly(GR), the level of Kapβ2 available is insufficient to prevent poly(GR) toxicity. Overexpressing Kapβ2 may be beneficial because it can bind the excess poly(GR) and bring the system back to a favorable balance for neuronal survival. While this work only explored TDP-43 nuclear localization, other toxic

mechanisms associated with poly(GR) (stress granules persistence, mitochondrial toxicity, etc. (Moens et al., 2019, Chew et al., 2019a, Choi et al., 2019)) may also rescue poly(GR) toxicity. This idea will need further evaluation in future works.

The results presented in this paper align with many other studies focused on DPR toxicity. Our studies showed an increase in the hazard ratio for neurons that produce DPRs. However, it is well-known that post-mortem tissues show a very low abundance of DPRs (Zu et al., 2013). Indeed, when we analyzed Kapβ2 expression in post-mortem tissues, we did not find perturbation of Kapβ2 levels. What has become apparent for C9-ALS is that there are multiple and non-exclusive toxic mechanisms at play during disease progression. In this respect, a Kapβ2-based therapeutic strategy might not be able to be a stand-alone treatment for ALS but might work in conjunction with drugs targeting other pathways. Kapβ2 levels could conceivably be raised in neurons using a therapeutic strategy based on genetic delivery of Kapβ2 into the central nervous system, using gene therapy strategies such as mRNA-nanoparticle technology (Hou et al., 2021). Future studies would also be directed to screening for compounds that can induce the expression of Kapβ2 in neurons. Another intriguing therapeutic possibility is *via* promoting arginine methylation. The Kapβ2-FUS interaction is modulated by FUS methylation status (Hofweber et al., 2018). Arginine methylation is a poly(GR) post-translational modification that sometimes dictates disease severity (Gittings et al., 2020). The most abundant poly(GR) methylation status in post-mortem tissues is the asymmetric di-methylated form, but poly(GR) can be present with symmetrical di-methylation or mono-methylation. It would be essential to expand on this concept and study how the different methylation status/conditions of poly(GR) influence Kapβ2 binding and, thus, poly(GR) toxicity.

In summary, we showed that manipulating Kapβ2 levels is beneficial against poly(GR) induced neurotoxicity. Future studies are needed to translate this concept into a therapeutic reality.

ACKNOWLEDGMENTS

We thank the members of the Jefferson Weinberg ALS Center for feedback throughout the development of this project. The following sources supported this work: National Institutes of

Health R21-NS090912 (D.T.), RF1-AG057882 (D.T.), R01-NS109150 (P.P.); Muscular Dystrophy Association grant 628389 (D.T.); DoD grant W81XWH-21-1-0134 (M.E.C.); RF1-NS114128 (A.H.); Family Strong for ALS & Farber Family Foundation (A.H., P.P., D.T.); R35GM138109 (L.G), Dr. Ralph and Marian Falk Medical Research Trust (L.G.), Frick Foundation for ALS Research (L.G)

AUTHOR CONTRIBUTION

M.E.C. and D.T. conceived the study, designed the experiments, interpreted the results, and wrote and revised the manuscript. D.T. supervised all the experiments and provided the resources for the project. M.E.C. performed the live-cell imaging experiments and the statistical analysis. S.S. performed FRAP experiments and analyzed the live-cell imaging data. V.K. performed the experiments in mouse tissues, the co-immunoprecipitations, and the TDP-43 localization experiments. B.M.V. managed the animal colony. S.M. performed the experiments with human samples. K.K. prepared primary neuronal cultures. A.B. performed Imaris analysis. L.G. and A.G. performed the experiments in the test tube and conducted data analysis. A.T.N. designed lentiviral plasmids and produced the virus. B.L.R performed light sheet sample preparation and acquisition.

DECLARATION OF INTEREST

The authors declare no competing financial interests.

MATERIALS AND METHODS

Cell cultures

HEK293 cells were cultured in DMEM medium (Cytiva Cat.# SH30243.LS) supplemented with 10% FBS (Cytiva Cat.# SH30071.01HI), penicillin, and streptomycin (Thermo Fisher Scientific Cat.# SV30010). Cells were passaged every 3-4 days using 0.05% trypsin (Corning Cat.# 25-051-C). For FRAP experiments, cells were plated in poly D-lysine coated 35 mm glass bottom dishes (Cellvis Cat.# D35-10-1.5-N) at 30,000 cells/well density.

Primary cortical neurons

Embryonic day 16 (E16) rat embryos were harvested, brains were dissected, and the meninges were removed. Cortices and midbrain regions were cut into small pieces with scissors and incubated on a shaker at 80 rcf for 45 min at 37°C in 0.2% trypsin in HBSS without Ca^{2+} and Mg^{2+} (Cytiva Cat.# SH30588.01). FBS (Cytiva Cat.# SH30071.01HI) was added, and the cell suspension was centrifuged at 800 rcf for 10 minutes at 4°C. Cells were washed with Ca^{2+} and Mg^{2+} free HBSS and centrifuged at 800 rcf for 10 minutes at 4°C. The cell suspension was then passed through a 70 μm strainer (Foxx Life Sciences Cat.# 410-0002-OEM) to remove undigested connective tissue and large cellular clumps. Dispersed cells were then counted and plated in poly-D lysine-coated plates. The following plating densities were used: 150,000 cells/well in 24 well plates; 300,000 cells/well in 12 well plates; 5,000,000 cells/dish in 10 cm dishes.

Animals

Flag-GR_{50}-GFP (GR_{50}-GFP) or Flag-GFP (control-GFP) mice were crossed with CAG-*Cre* mice to ensure constitutive expression of GR_{50}-GFP or control GFP. Mice at 12 months of age were sacrificed, and cortices and spinal cords were collected and frozen in liquid N_2 or embedded in OCT. Frozen samples were stored at -80°C till the time of processing.

Plasmids and siRNA

The following plasmids were used: pCDNA3_hSyn_Td_Tomato; pCDNA3_hU6_Flag_mCherry; pCDNA3_hU6_Flag_GR_{50}_mCherry; pCDNA3_hU6_Flag_GR_{100}_mCherry; pCDNA3_CMV_eGFP; pCDNA3_CMV_eGFP_Kapβ2.

eGFP and eGFP_Kapβ2 were co-transfected with Td_Tomato at a DNA concentration ration of 1:2 (200ng/400ng) or 1:4 (200ng/800ng). eGFP and eGFP_Kapβ2 were co-transfected with mCherry, mCherry_GR_{50} and mCherry_GR_{100} at 1:1 ratio (400ng/400ng).

Human TDP-43 and TDP-43-GFP were subcloned into pE-SUMO (LifeSensors, Malvern, PA) as described (McGurk et al., 2018). All plasmid inserts were fully sequenced and confirmed to be correct.

To silence Kapβ2, 50 μM of ON-TARGETplus siRNA - TNPO1 - Smart Pool (Horizon Discovery, L-086861-02-0005) was used. 50μM of AllStars Negative Control scramble siRNA (Qiagen Cat.# 1027280) was used as control.

Transfection

Lipofectamine 2000 (Fisher Scientific Cat.# 11-668-019) was used to transfect HEK cells and cortical neurons following manufacturer instruction (1 μL Lipo2000/500ng total DNA). HiPerfect Transfection Reagent (Qiagen Cat.# 301705) was used to transfect siRNA (8μL HiPerfect/50nM siRNA). siRNA was transfected 24h before plasmids transfection. For cortical neurons, Lipo/DNA or RNA mix was incubated with the neurons for 1h, and then cell media were changed with fresh ones. For HEK293 cells, the mixture was incubated with the cells overnight.

Lentivirus Production

HEK293 cells were transfected with the following plasmids: pLenti_hSyn_Flag_eGFP or pLenti_hSyn_Flag_GR_{50}_eGFP, psPAX2 (Addgene Plasmid #12260), pMD2.G (Addgene Plasmid #12259). Plasmids were diluted in DMEM, and Pei MAX was added as a transfection reagent. The mix was incubated with HEK293 cells confluent at 70% for 5h, the media was changed with a fresh one. Cells supernatant was collected 48h after transfection and centrifuged for 10 min at 2,000 rcf at 4°C. Lentivirus Concentrator (OriGene Technologies Cat.# TR30025) was added to the supernatant and incubated overnight at 4°C. To pellet the virus, the media was centrifuged at

500 rcf for 45 min at 4°C. Viral particles were then resuspended in Ca^{2+} and Mg^{2+} free PBS (Cytiva Cat.# SH30028.LS), aliquoted and immediately frozen in liquid N_2.

Purification of Recombinant Proteins

His_6-SUMO1 N-terminally tagged TDP-43-WT and TDP-43-GFP were purified as described (McGurk et al., 2018) and overexpressed in BL21(DE3)RIL *E.coli* cells. These cells were then sonicated on ice in 50 mM HEPES (pH 7.5), 2% TritonX-100, 300 mM NaCl, 30 mM imidazole, 5% glycerol, 2 mM β-mercaptoethanol, and protease inhibitors (cOmplete, EDTA-free, Roche). The recombinant TDP-43 proteins were purified over Ni-NTA agarose beads (Qiagen) and eluted using 50 mM HEPES (pH 7.5), 150 mM NaCl, 300 mM imidazole, 5% glycerol, and 5 mM DTT. The buffer was exchanged with the same buffer without imidazole. The eluate containing the recombinant TDP-43 proteins was then frozen in liquid N_2, and stored as aliquots at -80°C until use.

Kapβ2 was purified as described (Guo et al., 2018). In brief, *E. coli* BL21-CodonPlus(DE3)-RIL cells (Agilent) were transformed with GST-Tev-Kapβ2 plasmid, and expression was induced overnight at 25°C with 1 mM IPTG. Cells were pelleted and resuspended in Tris buffer (50 mM Tris pH 7.5, 100 mM NaCl, 1 mM EDTA, 20% (v/v) glycerol, 2 mM DTT, supplemented with protease inhibitors), then lysed by sonication. Cell lysate was then loaded onto glutathione Sepharose™ 4 Fast Flow resin (GE Healthcare), and washed with Tris buffer, followed by ATP buffer (50 mM Tris pH 7.5, 100 mM NaCl, 1 mM EGTA, 0.5 mM $MgCl_2$, 5 mM ATP, 20% glycerol, 2 mM DTT, supplemented with protease inhibitors), then washed and eluted with Buffer A (20 mM imidazole, 75 mM NaCl, 1 mM EDTA, 20% (v/v) glycerol, 2 mM DTT). Finally, the protein was cleaved with Tev protease and purified on a HiTrap Q HP column (GE Healthcare) using a salt gradient. Purified protein was concentrated, flash frozen, and stored at -80°C. Before the aggregation assay, the protein was thawed and centrifuged at 16,100 x *g* for 10 min to remove any preformed aggregates. Protein concentration was determined by Bradford assay (Bio-Rad, Hercules, CA).

Equimolar concentrations of Kapβ2 (5 μM), TDP-43 (5μM), and $(GR)_{20}$ (5μM) were used. 200nM HIS6-SUMO-TDP-43-GFP and 100nM TAMRA-$(GR)_{20}$ were added to visualize TDP-43 and $(GR)_{20}$.

Peptides

Chemically synthesized $(GR)_{20}$ and Tetramethylrhodamine (TAMRA)-tagged $(GR)_{20}$ were obtained as a lyophilized powder from Peptide2.0 and dissolved in 1XPBS.

Sample preparation

For human tissues: 100 mg of fresh frozen lumbar spinal cord samples were homogenized in 1% SDS using a 15ml Dounce Homogenizer. The homogenate was centrifuged at 3000 rcf for 20 minutes at 4°C to remove tissue debris. Using a BCA assay (Pierce BCA kit# 23225), protein estimation was performed on the clear homogenate. 30 μg of protein samples are loaded for Western blot analysis.

For mouse tissues: 50 mg of CNS tissues were chopped into small pieces, incubated in RIPA for 2 h, and homogenized by pipetting every 20/25 minutes. Samples were then sonicated using Bioruptor Pico - Diagenode.

For cell cultures: Cells were harvested in PBS and centrifuged at 500 rcf for 3 minutes. PBS was removed by suction, and samples were resuspended in 80 μL of RIPA with protease inhibitor (Sigma-Aldrich Cat# P2714-1BTL). Cells were incubated for 15 minutes at 4°C on an orbital shaker and then sonicated with Bioruptor Pico - Diagenode. After sonication, samples were centrifuged at 16,000 rcf for 5 minutes at 4°C. Supernatant was kept, and BCA was used to measure the protein content of each sample.

Western blot

Cell cultures and animal tissues: 15μg of protein extracts were loaded on 10% pre-cast gels (Bio-Rad Cat.# 4568034) and run for 1hr at 100V. Gels were then transferred on PVDF membrane (Millipore Cat.# IPVH00010) overnight at 4°C at 30V and developed with the indicated primary and secondary antibodies. Membranes were developed with SuperSignal™ West Femto Maximum Sensitivity Substrate (Thermo Fisher Scientific Cat# 34094), and images were acquired using ChemiDOC XRS+ System (Bio-Rad).

Human samples: The gels were UV activated for 5 minutes before transferring onto the 0.22 μm nitrocellulose membrane. The semi-dry transfer was done using a Trans-Blot Turbo Transfer System (Bio-Rad) at 25mV for 10 minutes. A stain-free blot image was captured after the transfer and used as total protein. The blot was processed as previously described for cell cultures and animal tissues. The quantification is done using Image Lab Software (Bio-Rad); the intensity of Kapβ2-positive band is normalized to its total protein.

Immunoprecipitation

Immunoprecipitation was carried out using anti-Flag agarose beads (mouse IgG agarose beads were used as control). Rat primary cortical neurons and tissues were extracted in IP buffer containing 50 mM Tris-HCl (pH 7.5), 150 mM NaCl, 1mM EDTA, 0.5% NP-40, 100 mM EDTA (pH 8.0) supplemented with protease inhibitor (Sigma-Aldrich Cat# P2714-1BTL). After incubating at 4°C for 30 min., the samples were sonicated and then centrifuged for 10 min. at 10,000 rcf. Bradford assay was used to determine protein concentration. The agarose beads were added to 600 μg of cell lysates and incubated at 4°C for 24h under constant shaking. Cell lysates were centrifuged for 1 min. at 1,000 rcf to collect the supernatant. The pellets were washed five times, but only the first wash was collected. After the last centrifugation, the samples were eluted with SDS-PAGE loading dye at 95°C for 5 min. The entire eluate was run for Western blot. 60 μg of total lysate was used as input.

Immunofluorescence

Primary cortical neurons were fixed for 20 minutes at 37°C with 4% PFA and incubated in PermBlock solution (2% BSA, 0.3% Triton-x, 5% donkey serum in PBS). Primary antibodies were diluted in 0.1% BSA. Cells were incubated with the specified primary antibody solution overnight at 4°C on an orbital shaker. The following day cells were washed two times with PBS at room temperature for 10 minutes and incubated with the appropriate secondary antibody for 1h at room temperature. Cells were then washed twice in PBS and incubated with Hoechst solution (Thermo Fisher Scientific Cat.# 62249) for 10 minutes at room temperature to stain the nuclei.

After a final rinse in PBS, coverslips were mounted on glass slides using AquaMount (Lerner Laboratories Cat.# 13800).

Tissues were cryo-sectioned using Cryostar NX50. 20 μm thick sections were placed on glass slides and incubated for 10 minutes in 4% PFA. Slides were then washed in TBS-T for 10 minutes and then incubated for 1h at room temperature in PermBlock solution (2% BSA, 0.3% Triton-x, 5% donkey serum in PBS), incubated with primary antibody diluted in 1% BSA, 0.3% Triton-x and 1% donkey serum overnight at 4°C in a humidified chamber. The following day, slides were washed with TBS-T, incubated with the appropriate fluorescent secondary antibody for 1 hour at room temperature, rinsed twice in TBS-T, incubated for 10 minutes with Hoechst (Thermo Fisher Scientific Cat.# 62249), and mounted on coverslips using AquaMount (Lerner Laboratories Cat.# 13800).

Antibodies and dilutions

Primary antibodies: anti-Kapβ2 (Santa Cruz Biotechnology, Inc Cat.# sc-101539; WB dilution 1:1000); anti-Kapβ2 (Sigma Cat.# T0825; IF dilution 1:500); anti-Map2 (Novus Biologicals Cat.# NB300-213; IF dilution 1:2000); anti-GFP (Proteintech Cat.# 50430-2-AP; WB dilution 1:1000); anti-TDP-43 (Proteintech Cat.# 22309-I-AP; IF dilution 1:500); anti-GAPDH (Proteintech Cat.# 60004-1-Ig; WB dilution 1:1000); anti-Vinculin (Invitrogen Cat.# 241794; WB dilution 1:500); Neun (D4G40) XP(Cell Signaling Technology Cat.# 24307; IF dilution 1:500)

Secondary HRP-conjugated antibodies: HRP-Conjugated anti-rabbit (Cytiva Cat.# NA9340-1ML; WB dilution 1:10,000); HRP-Conjugated anti-mouse (Cytiva Cat.# NA9310-1ML; WB dilution 1:10,000); HRP-Conjugated anti-rat (Sigma-Aldrich Cat.# AP136P; WB dilution 1:3,000);

Secondary fluorescent antibodies: AlexaFluor-546 anti-mouse (Life Technologies Cat.# A10036; IF dilution 1:1,000); AlexaFluor-647 anti-rabbit (Life Technologies Cat.# A31573; IF dilution 1:1,000); AlexaFluor-647 anti-chicken (Invitrogen Cat.# A32933; IF dilution 1:1,000);

Total RNA extraction and quantitative Real-Time PCR

Total RNA was extracted using Trizol Reagent (Ambion Cat.# 15596026) following the manufacturer's instructions. Briefly, cells were lysed in Trizol Reagent and homogenized using a

syringe for insulin. RNA was then extracted in isopropanol. Samples were centrifuged for 15 min. at 12,000 rcf. The RNA-containing pellet was washed with 75% ethanol and centrifuged for 5 min. at 7,500 rcf. Dried pellets were resuspended in DEPC water, and concentration was assessed with Nanodrop. 500ng of total RNA was first treated with DNAse I (Thermo Fisher Scientific Cat.# EN0521) and retrotranscribed using SuperScript™ IV Reverse Transcriptase (Thermo Fisher Scientific Cat.# 18090010). The cDNA was diluted 1:2 and used for qRT-PCR, which was performed using the following TaqMan assay: GAPDH-VIC (Thermo Fisher Scientific Cat# 4352338E) and Kapβ2-FAM (Thermo Fisher Scientific Cat.# 4331182 Assay# Rn01489969_m1). 50ng of cDNA was used per reaction. Samples were analyzed using Design and Analysis tool by Thermo Fisher Scientific. Results are shown as fold change using the $2^{\Delta\Delta Ct}$ method.

Whole brain immunolabeling, clearing, and light sheet microscopy.

For whole brain immunolabeling and clearing, an online published protocol was used (https://idisco.info). Briefly, fixed tissues undergo subsequent steps with a higher methanol percentage to be dehydrated. 4% hydrogen peroxide treatment overnight at 4° is used to bleach the tissue. The tissue is rehydrated and permeabilized for 2 days with 0.5% Tween 20. Incubation with primary antibody was performed at 37° for an entire week under constant shaking. The following primary antibodies concentration were used: Kapβ2 1:500 (Sigma Cat.# T0825), NeuN 1:1000 (Cell Signaling Technology Cat.# 24307). Secondaries also were kept for one week at 37° with constant shaking (Alexa-Fluor goat anti-mouse 546 and Alexa-Fluor anti-rabbit 647). The tissue was then dehydrated with increasing methanol gradients, delipidated with DCM and cleared with DBE. Images were acquired thanks to light sheet microscopy with Ultra Microscope Blaze (Miltenyi Biotec) at 4X and a 12X objective with a 2.5X zoom. Images were then composed and analyzed with Imaris Software 9.7.2.

Confocal Imaging Analysis

Confocal images were taken on a Nikon A1R confocal microscope with a 60X objective. Z-stacks were taken for each image. 0.2 μm Z-stacks were taken to perform colocalization studies and puncta counting using a built-in function in Imaris. One μm stacks were taken for TDP-43

nuclear intensity studies. Maximum intensity projection was then generated through a built-in function of the A1R analysis software. The nuclei of each co-transfected cell were selected as the region of interest, and TDP-43 intensity was assessed.

FRAP analysis was done in cells that were green (GFP or GFP-Kapβ2) and red (mCherry, GR_{50}-mCherry, GR_{100}-mCherry) fluorescent. Aggregates were selected as regions of interested and photobleached for 2 sec. with blue light with laser power at 100% power. Following photobleaching, images were continuously taken for 3 minutes and analyzed with Nikon A1R software. Fluorescence recovery intensity curves over were built using Prism GraphPad 9.0.

Time-lapse imaging

Cells were imaged every two days after transfection. 20× objective was used, and 25 fields/well were acquired. Only cells positives for both Kapβ2 and mCherry were counted. Cells were scored dead when they disappeared from the field of view, or clear signs of neurites fragmentation appeared. Kaplan Meier curves were then constructed in Prism GraphPad 9.0.

Visualization of TDP-43 Condensates

His_6-SUMO1-TDP-43 (5 uM) was incubated with equimolar concentration of $(GR)_{20}$ for 1 hour at room temperature in PBS. 200 nM His_6-SUMO1-TDP-43-GFP and 100 nM TAMRA-$(GR)_{20}$ were added to visualize TDP-43 and $(GR)_{20}$. The reaction mixture was incubated at room temperature for 1h, and then samples were spotted onto a coverslip and imaged by DIC and fluorescent microscopy using a Leica DMi8 Inverted microscope. To inhibit condensation, 5μM Kapβ2 was added at the beginning of the assay.

Statistical analysis

All experiments were performed at least 3 times ($n \geq 3$). At least 3 mice/group were used. For live-cell imaging, >150 neurons/condition were counted for each n. For colocalization, puncta counting, and TDP-43 intensity, ≥10 neurons/condition were counted for each n. For FRAP experiment, ≥5 cells/condition were analyzed for each n. When two groups were compared, t-student test was performed using the built-in function in Prism GraphPad 9.0. The Kaplan Meier

curves were compared by the log-rank and Cox proportional hazards tests, the statistical significance between curves was assessed with Cox (GraphPad software). For FRAP experiment, statistical differences between the curves were evaluated by curve analysis (one way ANOVA test) in Prism GraphPad 9.0.

FIGURE LEGENDS

Figure 1. Poly(GR) interacts and recruits Kapβ2 in neurons.

A. Confocal imaging of primary rat cortical neurons transduced with Flag-GFP (top row) or Flag-GR_{50}-GFP (bottom row) and stained for Kapβ2. Green is GFP; red is Kapβ2, and magenta is Map2. Imaris colocalization shows the amount of GFP colocalized with Kapβ2. Scale bar=10μm.
B. Graphs showing Pearson coefficient measured in each neuron transduced with GFP or GFP-GR_{50}. Data are represented as mean ± S.E.M. (Student t-test, $P<0.05$) (n=3, m>5 neurons)
C. Western blot of the immunoprecipitation assay performed in rat cortical neurons transduced with GFP or GFP-GR_{50}. Input lanes show the total lysate while Co-IP shows the protein co-precipitated with GFP or GFP-GR_{50}. Blots were probed for GFP and Kapβ2.
D. Western blot of the immunoprecipitation assay performed in the brain or spinal cord tissue of GFP or GFP-GR_{50} mice. Input lanes show the total lysate while Co-IP shows the protein co-precipitated with GFP or GFP-GR_{50}. Blots were probed for GFP and Kapβ2.
E. Confocal imaging of the brain and spinal cord tissues of GFP-GR_{50} mice stained for Kapβ2. Green is GFP; red is Kapβ2, and magenta is NeuN. Imaris colocalization shows the amount of GFP colocalized with Kapβ2. Scale bar 30μm.
F. Graphs showing Pearson coefficient measured in brain and spinal cord neurons of GFP-GR_{50} mice. Data are represented as mean ± S.E.M. (n=3, m>15 neurons)
G. Western blot of controls and C9-ALS patient's spinal cord extracts. Blot was probed for Kapβ2
H. Graphs showing quantification of Kapβ2 expression in controls and C9-ALS spinal cord extracts. Data are represented as mean ± S.E.M. (Student t-test, n.s.)

Figure 2. Silencing of Kapβ2 increases death risk in presence of poly(GR)

A. Graph showing quantification of Kapβ2 mRNA in primary neurons treated with Smart pool SiRNA 50 μM or scramble. Data are represented as mean ± S.E.M. n=3. (Student t-test, $P<0.05$)

B. Western blot showing Kapβ2 expression in neurons treated with Smart pool SiRNA 50 μM or scramble.

C. Graph showing Kapβ2 mRNA in primary neurons treated with Smart pool SiRNA 50 μM or scramble. Data are represented as mean ± S.E.M. n=3 (Student t-test, $P<0.05$)

D. Graph showing risk of death after seven days or neurons transfect siRNA Kapβ2 50 μM or scramble and GFP, GFP-GR_{50} or GFP-GR_{100}. n=3 for GFP and GFP-GR_{50}, n=2 for GFP-GR_{100}. Data are represented as mean ± S.E.M.

E. Representative images of censored neurons over time transfected with SiRNA Kapβ2 50μM or scramble and 200/400ng of Tm/GFP, GFP-GR_{50}, GFP-GR_{100}. Scale bar 20μm.

Figure 3. Increased expression of Kapβ2 does not affect neuronal viability

A. Left: Confocal imaging of primary neurons transfected with GFP- Kapβ2. Arrows indicate cytoplasmic puncta. Green is GFP, and blue is DAPI. Scale bar 5μm. Center: Imaris 3D rendering of GFP- Kapβ2 expression in primary rat cortical neurons. Right: magnification of Imaris rendering of GFP- Kapβ2 puncta around the nucleus. Scale bar 3μm.

B. Kaplan-Meier curves of time-lapse experiments on rat primary cortical neurons transfected with 200/400ng of Tm^+/ GFP- Kapβ2$^+$ (GFP used as control) per 150,000 cells. Neurons double positive Tm^+/GFP^+ were counted (n=3, m>150 neurons). (Log-rank Mantel-Cox test: n.s.)

C. Representative images of censored neurons over time transfected with 200/400ng of Tm/GFP. Green is Kapβ2; red is Td-Tomato. Scale bar 20μm.

D. Kaplan-Meier curves of time-lapse experiments on rat primary cortical neurons transfected with 200/800ng of Tm^+/GFP- Kapβ2$^+$ (GFP used as control) per 150,000 cells. Neurons double positive Tm^+/GFP^+ were counted (n=3, m>150 neurons). (Log-rank Mantel-Cox test: n.s.)

E. Representative images of censored neurons over time transfected with 200/400ng of Tm^+/GFP^+. Green is Kapβ2; red is Td-Tomato. Scale bar 20μm.

Figure 4. Increased expression of Kapβ2 mitigates poly (GR) neuronal toxicity.

A. Confocal analysis of neuron overexpressing Kapβ2 and GR_{50}-mCherry (top row) or GR_{100}-mCherry (bottom row). Green is GFP; red is mCherry, and blue is DAPI. Imaris rendering is used to visualize the interaction of GFP- Kapβ2 and poly(GR)s-mCherry. Scale bar 5 μm.

B. Pearson coefficient analysis of GFP- Kapβ2 and GR_{50}-mCherry or GR_{100}-mCherry. Data are represented as mean ± S.E.M. (Student t-test, $P<0.05$)

C. Confocal analysis of neuron overexpressing Kapβ2 and GR_{50}-mCherry (top row) or GR_{100}-mCherry (bottom row). Green is GFP; red is mCherry, and blue is DAPI. The white line represents the length over which GFP and mCherry fluorescence were analyzed. Scale bar 10 μm.

D. Intensity profiles are plotted as GFP or mCherry fluorescence (a.u.) over distance (μm).

E. Kaplan-Meier curves of time-lapse experiments on rat primary cortical neurons transfected with 400/400ng of GFP-Kapβ2$^+$ (GFP alone used as control) and GR_{50}-mCherry (mCherry alone used as control) per 150,000 cells. Neurons double positive GFP$^+$/mCherry$^+$ were counted (n=3, m>150 neurons). (Log-rank Mantel-Cox test: mCherry vs mCherry-GR_{50} $p<0.0001$; mCherry-GR_{50} vs mCherry-GR_{50}/GFP- Kapβ2 $p<0.0001$). Inset: graph bar showing quantification of GR_{50}-mCherry and GR_{50}-mCherry-GFP- Kapβ2 overall survival normalized to mCherry 7 days post-transfection, n=3. Data are represented as mean ± S.E.M.

F. Kaplan-Meier curves of time-lapse experiments on rat primary cortical neurons transfected with 400/400ng of GFP- Kapβ2$^+$ (GFP alone used as control) and GR_{100}-mCherry (mCherry alone used as control) per 150,000 cells. Neurons double positive GFP$^+$/mCherry$^+$ were counted (n=3, m>150 neurons). (Log-rank Mantel-Cox test: mCherry vs mCherry-GR_{100} $p<0.0001$; GR_{100}-mCherry vs GR_{100}-mCherry/ Kapβ2 $p=0.005$). Inset: graph bar showing quantification of GR_{50}-mCherry and GR_{50}-mCherry-GFP- Kapβ2 overall survival normalized to mCherry 7 days post-transfection, n=3. Data are represented as mean ± S.E.M.

Figure 5. Kapβ2 does not change the dynamic properties of poly(GR)s aggregates.

A. mCherry (blue line) vs mCherry/GFP-Kapβ2 (black line). Percentage of recovered fluorescence plotted against time. (Two-ways ANOVA P= n.s.)

B. Representative images of the bleached aggregates at the start (sec=0), bleaching (sec=5), and end (sec=180). Scale bar 10 μm. Upper panels represent mCherry alone; middle and lower panels represent mCherry and GFP-Kapβ2 in the same cell. n=3, m>15 cells

C. mCherry-GR_{50} (red line) vs. mCherry-GR_{50}/GFP-Kapβ2 (black line). Percentage of recovered fluorescence plotted against time. (Two-ways ANOVA P= n.s.)

D. Representative images of the bleached aggregates at the start (sec=0), bleaching (sec=5), and end (sec=180). Scale bar 10 μm. Upper panels represent mCherry-GR_{50} alone; middle and lower panels represent mCherry-GR_{50} and GFP- Kapβ2 in the same cell. n=3, m>15 cells

E. mCherry-GR_{100} (blue line) vs mCherry-GR_{100}/GFP- Kapβ2 (black line). Percentage of recovered fluorescence plotted against time (Two-ways ANOVA P= n.s.).

F. Representative images of the bleached aggregates at the start (sec=0), bleaching (sec=5), and end (sec=180). Scale bar 10 μm. Upper panels represent mCherry-GR_{100} alone; middle and lower panels represent mCherry-GR_{100} and GFP- Kapβ2 in the same cell. n=3, m>15 cells

Figure 6. Increasing Kapβ2 expression levels leads to TDP-43 nuclear retention in the presence of poly(GR)

A. Confocal analysis of neuron overexpressing GFP or Kapβ2 and mCherry-GR_{50} or mCherry-GR_{100} (top row) or GR_{100}-mCherry (bottom row). Green is GFP, red is mCherry, magenta is TDP-43, blue is Hoechst. Scale bar 5 μm.

B. Graphs showing single-nuclei TDP-43 staining quantification. Data are represented as mean ± S.E.M. Only double positive cells were taken into consideration. (n=2, m>10 neurons). (Student t-test, P<0.01; P<0.001)

C. Epifluorescence images of condensates formation in presence of TDP-43, $(GR)_{20}$ and Kapβ2. Green is TDP-43, red is GR_{20}. Scale bar: 15μm.

D. Graph showing quantification of the size of TDP-43/GR20 aggregates in presence or absence of Kapβ2. n=3, data are represented as mean ± S.E.M. (Student t-test, P<0.01)

E. Graph showing the ratio between the mean GFP intensity inside and outside TDP-43/GR20 aggregates in the presence or absence of Kapβ2. n=3, data are represented as mean ± S.E.M. (Student t-test, P<0.0001)

Supplementary Figure 1

A. Western blot of the immunoprecipitation assay performed in rat cortical neurons transduced with GFP or GR_{50}-GFP.
B. Light sheet microscopy of GFP-GR_{50} mouse cortices. Left panel is 4X magnification, (scale bar 50μm) central and right panel are 12.5X magnification with a 2.5X optical zoom (scale bar 30 and 20 μm). Green is GFP,red in Kapβ2 and far red is NeuN.

Supplementary Figure 2

A. Graph showing quantification of Kapβ2 expression in brains (input) of GFP and GR_{50}-GFP animals
B. Graph showing quantification of Kapβ2 expression in spinal cords (input) of GFP and GR_{50}-GFP animals
C. Western blot of the immunoprecipitation assay performed on GR_{50}-GFP mouse brain. The left half of the blot show immunoprecipitation performed with ant-Flag beads. The right half of the blot shows mock immunoprecipitation performed with anti-mouse Igg beads.
D. Western blot of the immunoprecipitation assay performed on GR_{50}-GFP mouse spinal cord. The left half of the blot show immunoprecipitation performed with ant-Flag beads. The right half of the blot shows mock immunoprecipitation performed with anti-mouse IgG beads.

Supplementary Figure 3

A. Upper inset: confocal imaging of WT mouse spinal cord. Red is Kapβ2; far red is NeuN. Lower inset Imaris rendering of Kapβ2 staining in WT mouse spinal cord.

REFERENCES

CHEW, J., COOK, C., GENDRON, T. F., JANSEN-WEST, K., ROSSO, G., DAUGHRITY, L. M., CASTANEDES-CASEY, M., KURTI, A., STANKOWSKI, J. N., DISNEY, M. D., ROTHSTEIN, J. D., DICKSON, D. W., FRYER, J. D., ZHANG, Y.-J. & PETRUCELLI, L. 2019b. Aberrant deposition of stress granule- resident proteins linked to C9orf72 - associated TDP-43 proteinopathy. *Mol Neurodegener.* Molecular Neurodegeneration.

CHOI, S. Y., R, L.-G., G, K., HL, P., A, N. L., WW, S., WD, Y., S, A. & F-B, G. 2019. C9ORF72-ALS/FTD-associated poly(GR) binds ATP5 alpha1 and compromises mitochondria function in vivo. *Nature neuroscience*.

COOK, C. N., WU, Y., ODEH, H. M., GENDRON, T. F., JANSEN-WEST, K., DEL ROSSO, G., YUE, M., JIANG, P., GOMES, E., TONG, J., DAUGHRITY, L. M., AVENDANO, N. M., CASTANEDES-CASEY, M., SHAO, W., OSKARSSON, B., TOMASSY, G. S., MCCAMPBELL, A., RIGO, F., DICKSON, D. W., SHORTER, J., ZHANG, Y.-J. & PETRUCELLI, L. 2020. C9orf72 poly(GR) aggregation induces TDP-43 proteinopathy. *Science translational medicine.*

COYNE, A. N., ZAEPFEL, B. L., HAYES, L., FITCHMAN, B., SALZBERG, Y., LUO, E. C., BOWEN, K., TROST, H., AIGNER, S., RIGO, F., YEO, G. W., HAREL, A., SVENDSEN, C. N., SAREEN, D. & ROTHSTEIN, J. D. 2020. G4C2 Repeat RNA Initiates a POM121-Mediated Reduction in Specific Nucleoporins in C9orf72 ALS/FTD. *Neuron.* Elsevier Inc.

DEJESUS-HERNANDEZ, M., MACKENZIE, I. R., BOEVE, B. F., BOXER, A. L., BAKER, M., RUTHERFORD, N. J., NICHOLSON, A. M., FINCH, N. A., FLYNN, H., ADAMSON, J., KOURI, N., WOJTAS, A., SENGDY, P., HSIUNG, G. Y., KARYDAS, A., SEELEY, W. W., JOSEPHS, K. A., COPPOLA, G., GESCHWIND, D. H., WSZOLEK, Z. K., FELDMAN, H., KNOPMAN, D. S., PETERSEN, R. C., MILLER, B. L., DICKSON, D. W., BOYLAN, K. B., GRAFF-RADFORD, N. R. & RADEMAKERS, R. 2011. Expanded GGGGCC hexanucleotide repeat in noncoding region of C9ORF72 causes chromosome 9p-linked FTD and ALS. *Neuron,* 72**,** 245-256.

FELDMAN, E. L., GOUTMAN, S. A., PETRI, S., MAZZINI, L., SAVELIEFF, M. G., SHAW, P. J. & SOBUE, G. 2022. Amyotrophic lateral sclerosis. *Lancet*.

GENDRON, T. F. & PETRUCELLI, L. 2017. Disease Mechanisms of C9ORF72 Repeat Expansions.

GITTINGS, L. M., BOEYNAEMS, S., LIGHTWOOD, D., CLARGO, A., TOPIA, S., NAKAYAMA, L., TROAKES, C., MANN, D. M. A., GITLER, A. D., LASHLEY, T. & ISAACS, A. M. 2020. Symmetric dimethylation of poly-GR correlates with disease duration in C9orf72 FTLD and ALS and reduces poly-GR phase separation and toxicity. *Acta Neuropathologica,* 139**,** 407-410.

GLEIXNER, A. M., VERDONE, B. M., OTTE, C. G., ANDERSON, E. N., RAMESH, N., SHAPIRO, O. R., GALE, J. R., MAUNA, J. C., MANN, J. R., COPLEY, K. E., DALEY, E. L., ORTEGA, J. A., CICARDI, M. E., KISKINIS, E., KOFLER, J., PANDEY, U. B., TROTTI, D. & DONNELLY, C. J. 2022. NUP62 localizes to ALS/FTLD pathological assemblies and contributes to TDP-43 insolubility. *Nat Commun,* 13**,** 3380.

GONZALEZ, A., MANNEN, T., ÇAĞATAY, T., FUJIWARA, A., MATSUMURA, H., NIESMAN, A. B., BRAUTIGAM, C. A., CHOOK, Y. M. & YOSHIZAWA, T. 2021. Mechanism of karyopherin-β2 binding and nuclear import of ALS variants FUS(P525L) and FUS(R495X). *Scientific Reports.* Nature Publishing Group UK.

GUO, L., FARE, C. M. & SHORTER, J. 2019. Therapeutic Dissolution of Aberrant Phases by Nuclear-Import Receptors. *Trends in Cell Biology.* Elsevier Ltd.

GUO, L., KIM, H. J., WANG, H., MONAGHAN, J., FREYERMUTH, F., SUNG, J. C., O'DONOVAN, K., FARE, C. M., DIAZ, Z., SINGH, N., ZHANG, Z. C., COUGHLIN, M., SWEENY, E. A., DESANTIS, M. E., JACKREL, M. E., RODELL, C. B., BURDICK, J. A., KING, O. D., GITLER, A. D., LAGIER-TOURENNE, C., PANDEY, U. B., CHOOK, Y. M., TAYLOR, J. P. & SHORTER, J. 2018. Nuclear-Import Receptors Reverse Aberrant Phase Transitions of RNA-Binding Proteins with Prion-like Domains. *Cell,* 173**,** 677-692.e20.

HAYES, L. R., DUAN, L., BOWEN, K., KALAB, P. & ROTHSTEIN, J. D. 2020. C9orf72 arginine-rich dipeptide repeat proteins disrupt karyopherin-mediated nuclear import. *eLife.*

HOFWEBER, M., HUTTEN, S., BOURGEOIS, B., SPREITZER, E., NIEDNER-BOBLENZ, A., SCHIFFERER, M., RUEPP, M. D., SIMONS, M., NIESSING, D., MADL, T. & DORMANN, D. 2018. Phase Separation of FUS Is Suppressed by Its Nuclear Import Receptor and Arginine Methylation. *Cell,* 173**,** 706-719.e13.

HOU, X., ZAKS, T., LANGER, R. & DONG, Y. 2021. Lipid nanoparticles for mRNA delivery. *Nature Reviews Materials,* 6**,** 1078-1094.

HUTTEN, S., USLUER, S., BOURGEOIS, B., SIMONETTI, F., ODEH, H. M., FARE, C. M., CZUPPA, M., HRUSKA-PLOCHAN, M., HOFWEBER, M., POLYMENIDOU, M., SHORTER, J., EDBAUER, D., MADL, T. & DORMANN, D. 2020a. Nuclear Import Receptors Directly Bind to Arginine-Rich Dipeptide Repeat Proteins and Suppress Their Pathological Interactions. *Cell Reports,* 33**,** 108538.

LEE, K.-H., ZHANG, P., KIM, H. J., MITREA, D. M., SARKAR, M., FREIBAUM, B. D., CIKA, J., COUGHLIN, M., MESSING, J., MOLLIEX, A., MAXWELL, B. A., KIM, N. C., TEMIROV, J., MOORE, J., KOLAITIS, R.-M., SHAW, T. I., BAI, B., PENG, J., KRIWACKI, R. W. & TAYLOR, J. P. 2016. C9orf72 Dipeptide Repeats Impair the Assembly, Dynamics, and Function of Membrane-Less Organelles. *Cell.* Elsevier.

MAOR-NOF, M., SHIPONY, Z., LOPEZ-GONZALEZ, R., YOKOYAMA, J. S., PETRUCELLI, L., GITLER, A. D., MAOR-NOF, M., SHIPONY, Z., LOPEZ-GONZALEZ, R., NAKAYAMA, L., ZHANG, Y.-J. & COUTHOUIS, J. 2020. Article p53 is a central regulator driving neurodegeneration caused by C9orf72 poly (PR) Article p53 is a central regulator driving neurodegeneration caused by C9orf72 poly (PR). *Cell.* Elsevier Inc.

MCGURK, L., GOMES, E., GUO, L., MOJSILOVIC-PETROVIC, J., TRAN, V., KALB, R. G., SHORTER, J. & BONINI, N. M. 2018. Poly(ADP-Ribose) Prevents Pathological Phase Separation of TDP-43 by Promoting Liquid Demixing and Stress Granule Localization. *Mol Cell,* 71**,** 703-717 e9.

MOENS, T. G., NICCOLI, T., WILSON, K. M., ATILANO, M. L., BIRSA, N., GITTINGS, L. M., HOLBLING, B. V., DYSON, M. C., THOENG, A., NEEVES, J., GLARIA, I., YU, L., BUSSMANN, J., STORKEBAUM, E., PARDO, M., CHOUDHARY, J. S., FRATTA, P., PARTRIDGE, L. & ISAACS, A. M. 2019. C9orf72 arginine-rich dipeptide proteins interact with ribosomal proteins in vivo to induce a toxic translational arrest that is rescued by eIF1A. *Acta Neuropathologica.*

NEUMANN, M., VALORI, C. F., ANSORGE, O., KRETZSCHMAR, H. A., MUNOZ, D. G., KUSAKA, H., YOKOTA, O., ISHIHARA, K., ANG, L. C., BILBAO, J. M. & MACKENZIE, I. R. A. 2012. Transportin 1 accumulates specifically with FET proteins but no other transportin cargos

in FTLD-FUS and is absent in FUS inclusions in ALS with FUS mutations. *Acta Neuropathologica.*

RENTON, A. E., MAJOUNIE, E., WAITE, A., SIMÓN-SÁNCHEZ, J., ROLLINSON, S., GIBBS, J. R., SCHYMICK, J. C., LAAKSOVIRTA, H., VAN SWIETEN, J. C., MYLLYKANGAS, L., KALIMO, H., PAETAU, A., ABRAMZON, Y., REMES, A. M., KAGANOVICH, A., SCHOLZ, S. W., DUCKWORTH, J., DING, J., HARMER, D. W., HERNANDEZ, D. G., JOHNSON, J. O., MOK, K., RYTEN, M., TRABZUNI, D., GUERREIRO, R. J., ORRELL, R. W., NEAL, J., MURRAY, A., PEARSON, J., JANSEN, I. E., SONDERVAN, D., SEELAAR, H., BLAKE, D., YOUNG, K., HALLIWELL, N., CALLISTER, J. B., TOULSON, G., RICHARDSON, A., GERHARD, A., SNOWDEN, J., MANN, D., NEARY, D., NALLS, M. A., PEURALINNA, T., JANSSON, L., ISOVIITA, V. M., KAIVORINNE, A. L., HÖLTTÄ-VUORI, M., IKONEN, E., SULKAVA, R., BENATAR, M., WUU, J., CHIÒ, A., RESTAGNO, G., BORGHERO, G., SABATELLI, M., HECKERMAN, D., ROGAEVA, E., ZINMAN, L., ROTHSTEIN, J. D., SENDTNER, M., DREPPER, C., EICHLER, E. E., ALKAN, C., ABDULLAEV, Z., PACK, S. D., DUTRA, A., PAK, E., HARDY, J., SINGLETON, A., WILLIAMS, N. M., HEUTINK, P., PICKERING-BROWN, S., MORRIS, H. R., TIENARI, P. J. & TRAYNOR, B. J. 2011. A hexanucleotide repeat expansion in C9ORF72 is the cause of chromosome 9p21-linked ALS-FTD. *Neuron,* 72**,** 257-268.

SCHLUDI, M. H., MAY, S., GRÄSSER, F. A., RENTZSCH, K., KREMMER, E., KÜPPER, C., KLOPSTOCK, T., CEBALLOS-BAUMANN, A., DANEK, A., DIEHL-SCHMID, J., FASSBENDER, K., FÖRSTL, H., KORNHUBER, J., OTTO, M., DIETERICH, M., FEUERECKER, R., GIESE, A., KLÜNEMANN, H., KURZ, A., LEVIN, J., LORENZL, S., MEYER, T., NÜBLING, G. & ROEBER, S. 2015. Distribution of dipeptide repeat proteins in cellular models and C9orf72 mutation cases suggests link to transcriptional silencing. *Acta Neuropathologica,* 130**,** 537-555.

STEWART, M. 2007. Molecular mechanism of the nuclear protein import cycle. *Nature Reviews Molecular Cell Biology.*

TAKEUCHI, R., TOYOSHIMA, Y., TADA, M., SHIGA, A., TANAKA, H., SHIMOHATA, M., KIMURA, K., MORITA, T., KAKITA, A., NISHIZAWA, M. & TAKAHASHI, H. 2013. Transportin 1 accumulates in FUS inclusions in adult-onset ALS without FUS mutation. *Neuropathology and Applied Neurobiology.*

TROAKES, C., HORTOBÁGYI, T., VANCE, C., AL-SARRAJ, S., ROGELJ, B. & SHAW, C. E. 2013. Transportin 1 colocalization with Fused in Sarcoma (FUS) inclusions is not characteristic for amyotrophic lateral sclerosis-FUS confirming disrupted nuclear import of mutant FUS and distinguishing it from frontotemporal lobar degeneration with FUS inclusi. *Neuropathology and Applied Neurobiology.*

TWYFFELS, L., GUEYDAN, C. & KRUYS, V. 2014. Transportin-1 and Transportin-2: Protein nuclear import and beyond. *FEBS Letters.* Federation of European Biochemical Societies.

VERDONE, B. M., CICARDI, M. E., WEN, X., SRIRAMOJI, S., RUSSELL, K., MARKANDAIAH, S. S., JENSEN, B. K., KRISHNAMURTHY, K., HAEUSLER, A. R., PASINELLI, P. & TROTTI, D. 2022. A mouse model with widespread expression of the C9orf72-linked glycine-arginine dipeptide displays non-lethal ALS/FTD-like phenotypes. *Sci Rep,* 12**,** 5644.

WEN, X., TAN, W., WESTERGARD, T., KRISHNAMURTHY, K., MARKANDAIAH, S. S., SHI, Y., LIN, S., SHNEIDER, N. A., MONAGHAN, J., PANDEY, U. B., PASINELLI, P., ICHIDA, J. K. & TROTTI, D. 2014a. Antisense proline-arginine RAN dipeptides linked to C9ORF72-ALS/FTD form

toxic nuclear aggregates that initiate invitro and invivo neuronal death. *Neuron.* Elsevier Inc.

XUE, Y. C., NG, C. S., XIANG, P., LIU, H., ZHANG, K., MOHAMUD, Y. & LUO, H. 2020. Dysregulation of RNA-Binding Proteins in Amyotrophic Lateral Sclerosis. *Front Mol Neurosci,* 13**,** 78.

ZHANG, K., DONNELLY, C. J., HAEUSLER, A. R., GRIMA, J. C., MACHAMER, J. B., STEINWALD, P., DALEY, E. L., MILLER, S. J., CUNNINGHAM, K. M., VIDENSKY, S., GUPTA, S., THOMAS, M. A., HONG, I., CHIU, S. L., HUGANIR, R. L., OSTROW, L. W., MATUNIS, M. J., WANG, J., SATTLER, R., LLOYD, T. E. & ROTHSTEIN, J. D. 2015. The C9orf72 repeat expansion disrupts nucleocytoplasmic transport. *Nature,* 525**,** 56-61.

ZU, T., LIU, Y., BAÑEZ-CORONEL, M., REID, T., PLETNIKOVA, O., LEWIS, J., MILLER, T. M., HARMS, M. B., FALCHOOK, A. E., SUBRAMONY, S. H., OSTROW, L. W., ROTHSTEIN, J. D., TRONCOSO, J. C. & RANUM, L. P. W. 2013. RAN proteins and RNA foci from antisense transcripts in C9ORF72 ALS and frontotemporal dementia. *Proceedings of the National Academy of Sciences,* 110**,** E4968-E4977.

Fig. 1

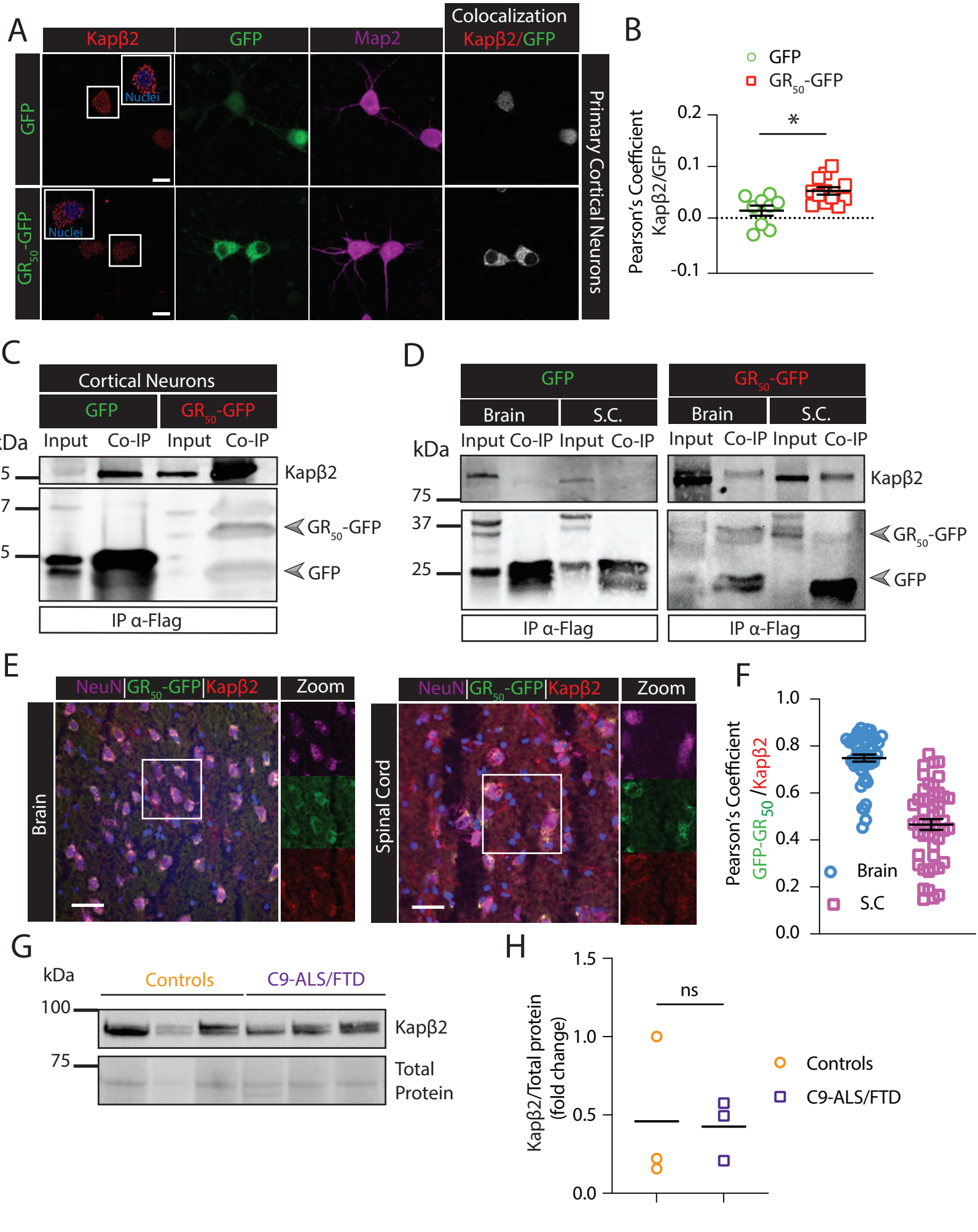

Fig. 2

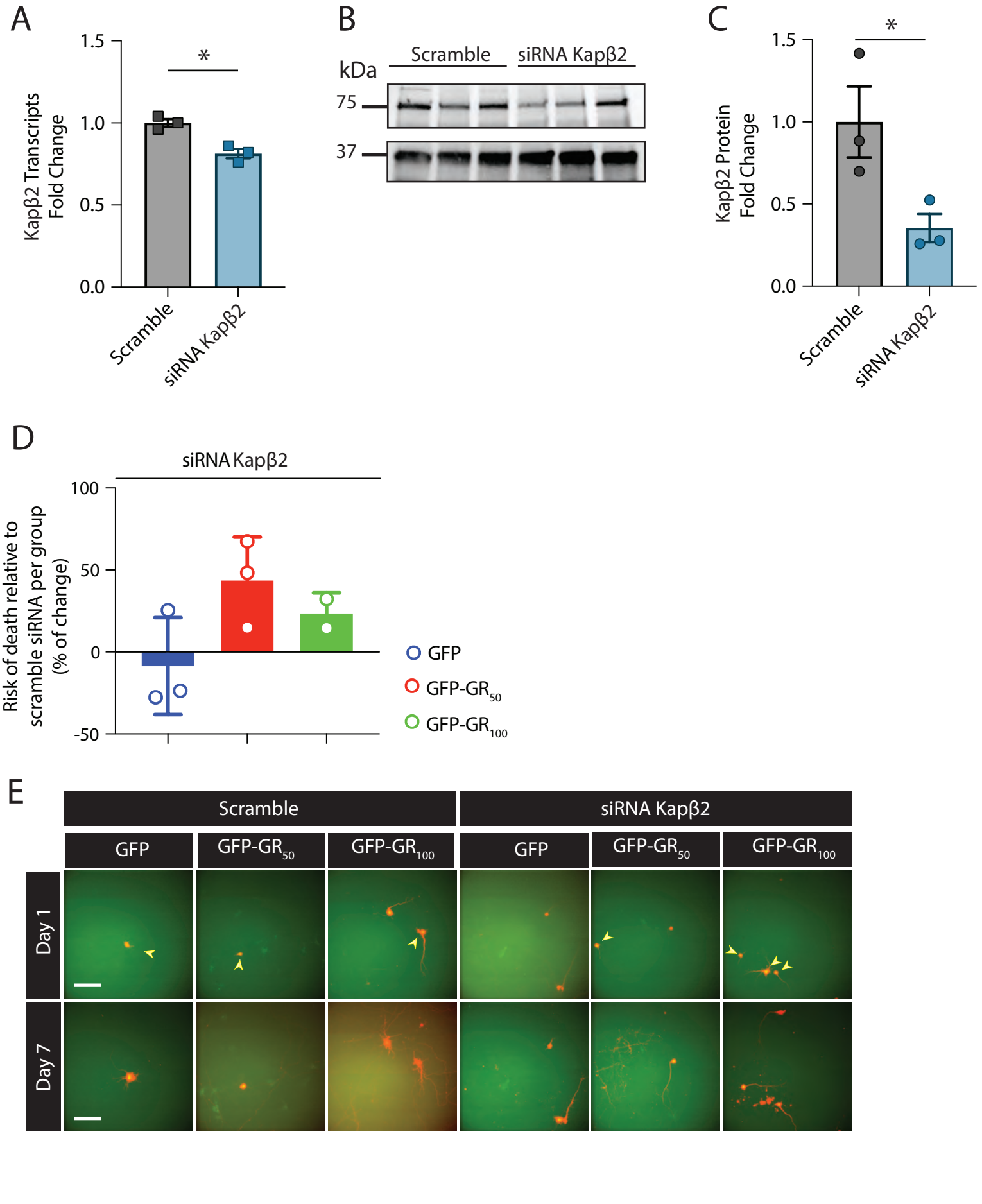

Fig. 3

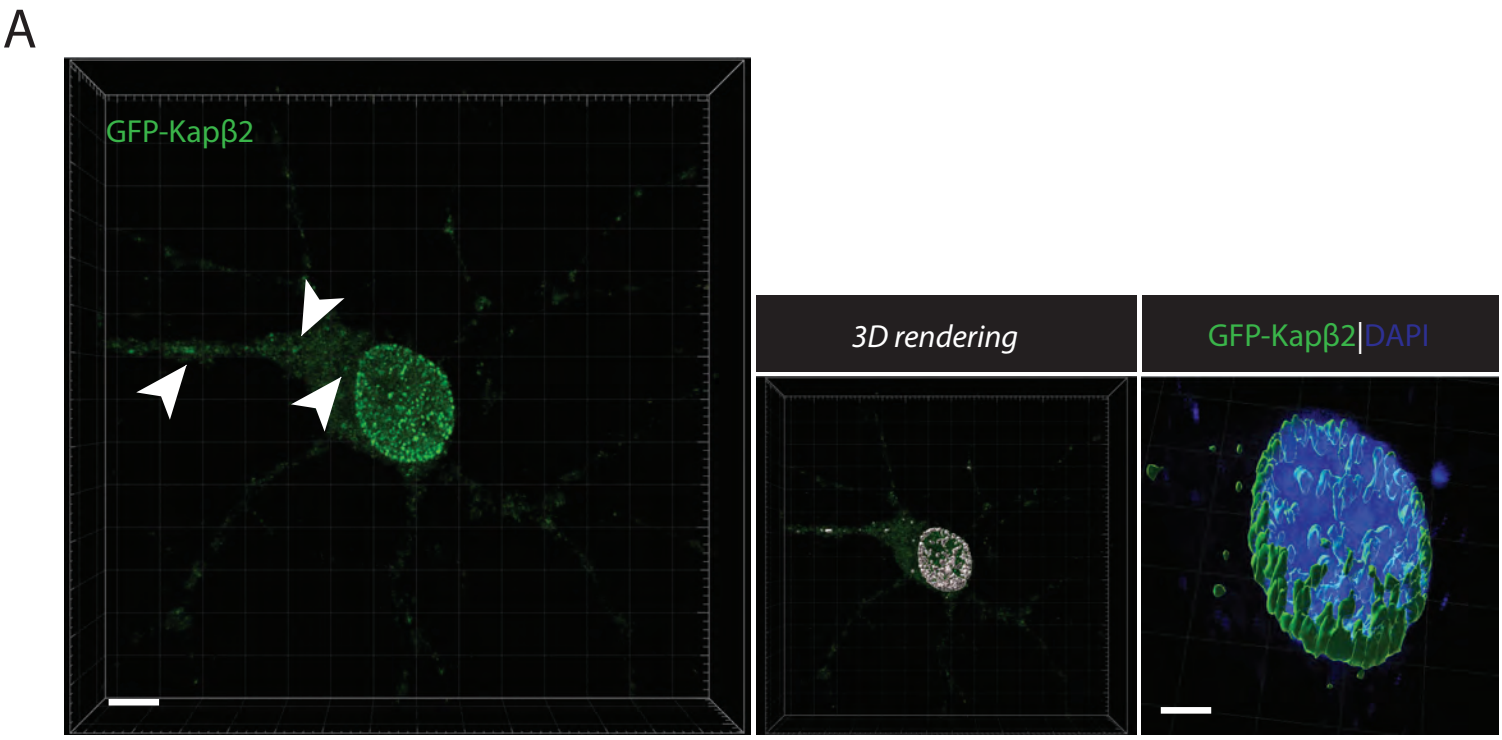

Fig. 4

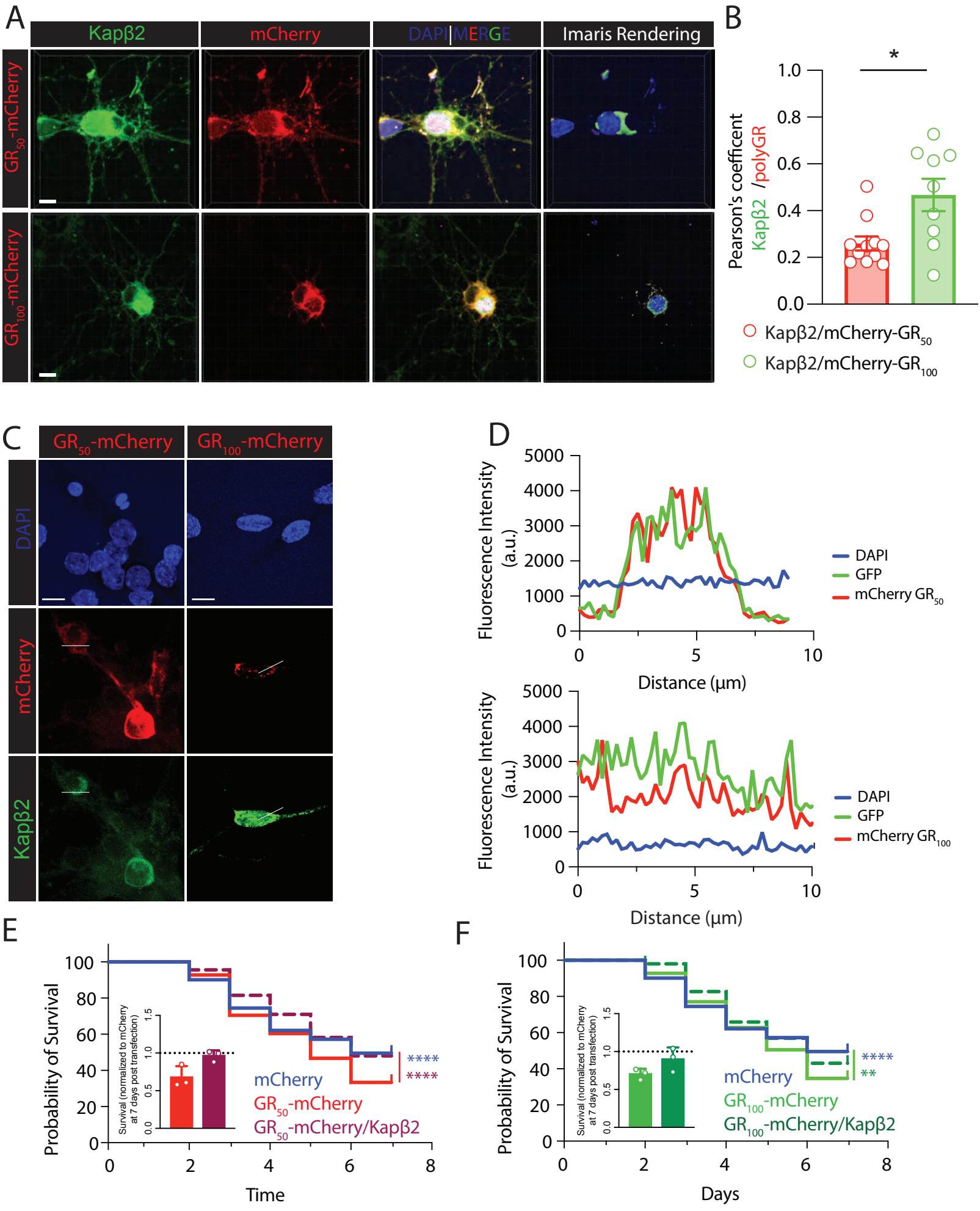

Fig. 5

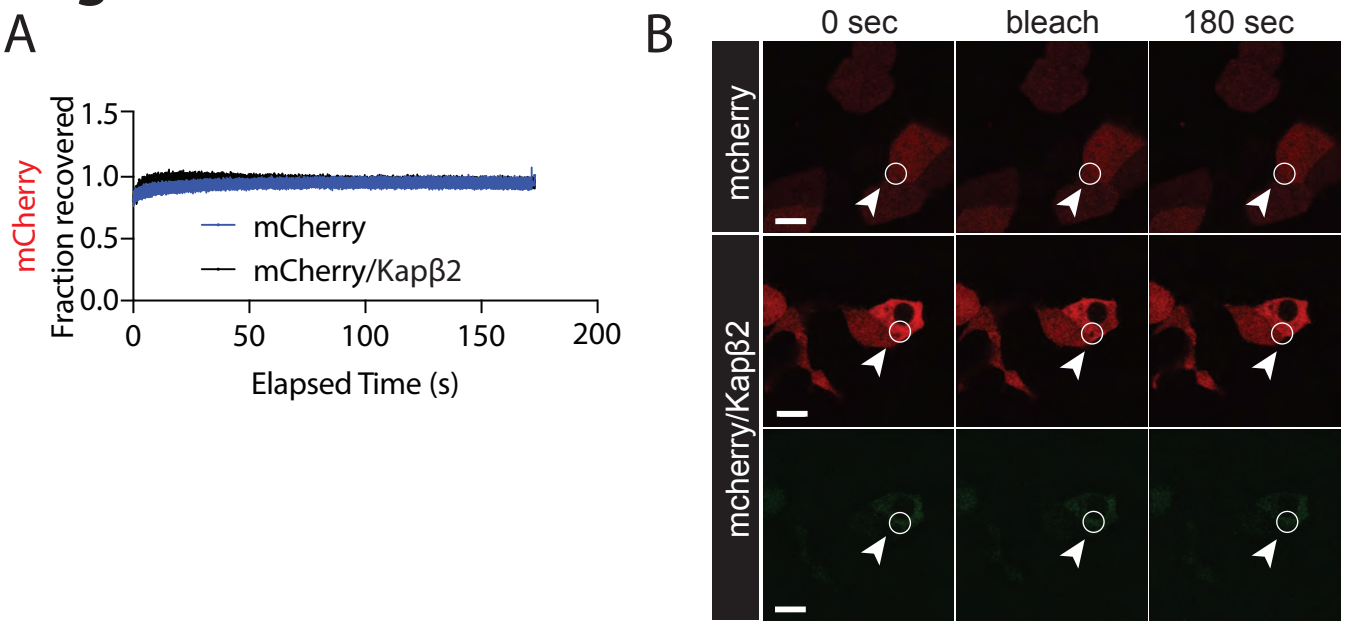

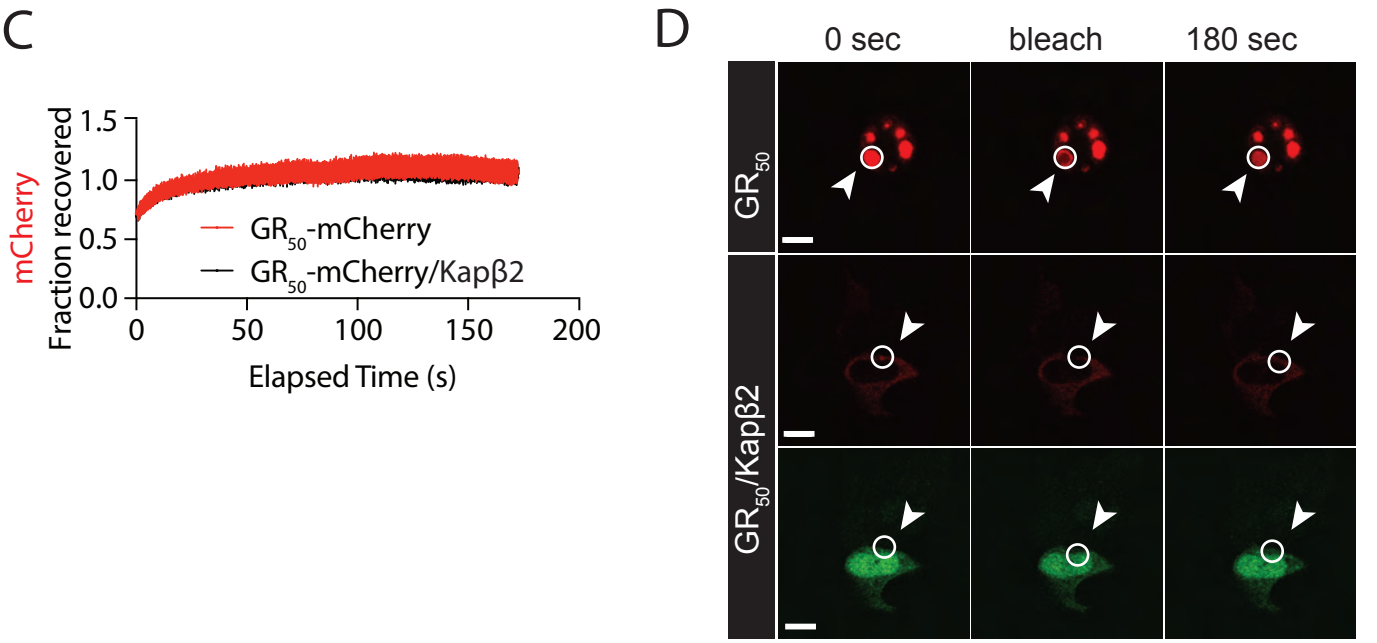

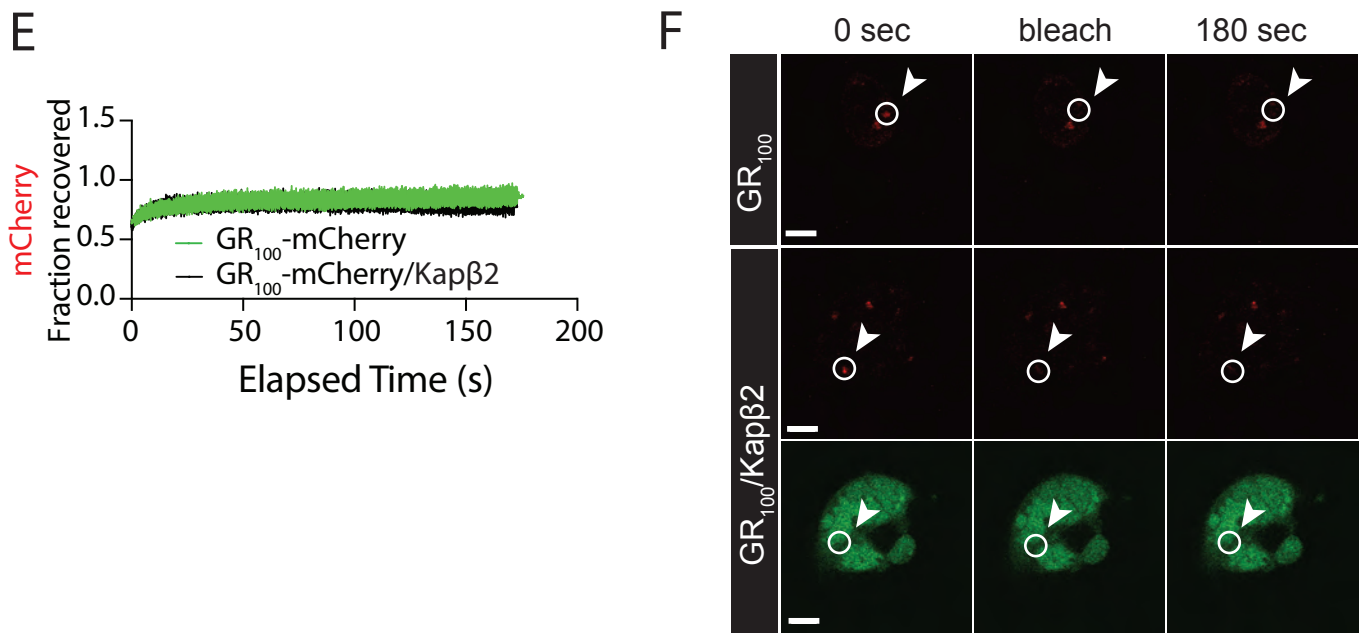

Fig. 6

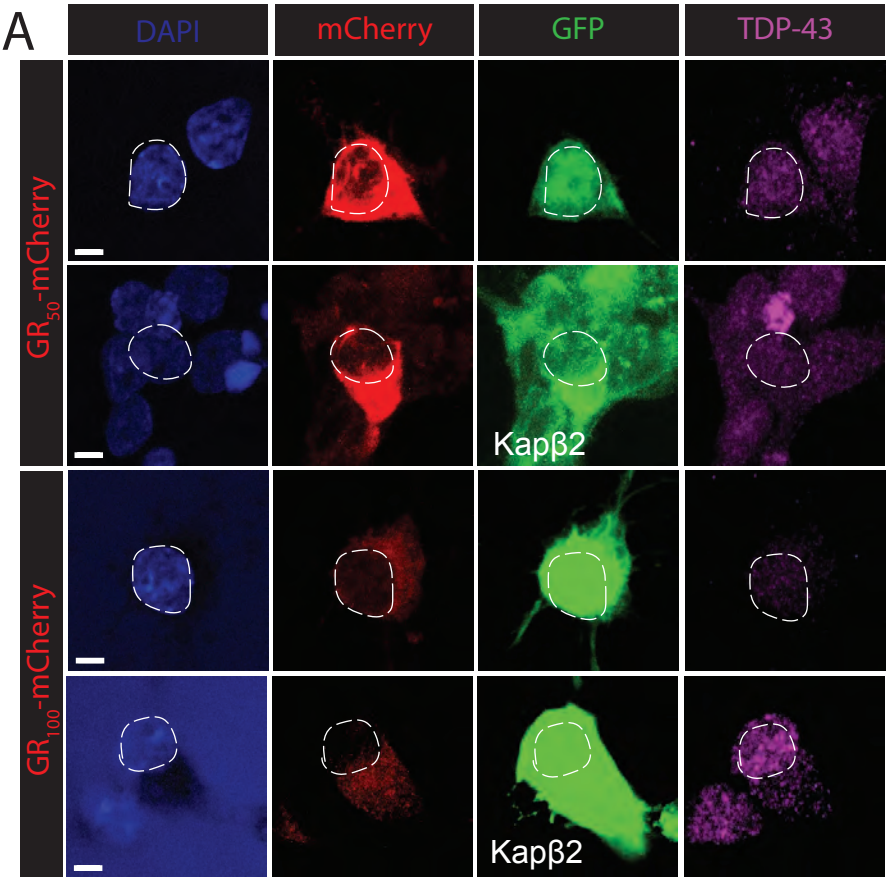

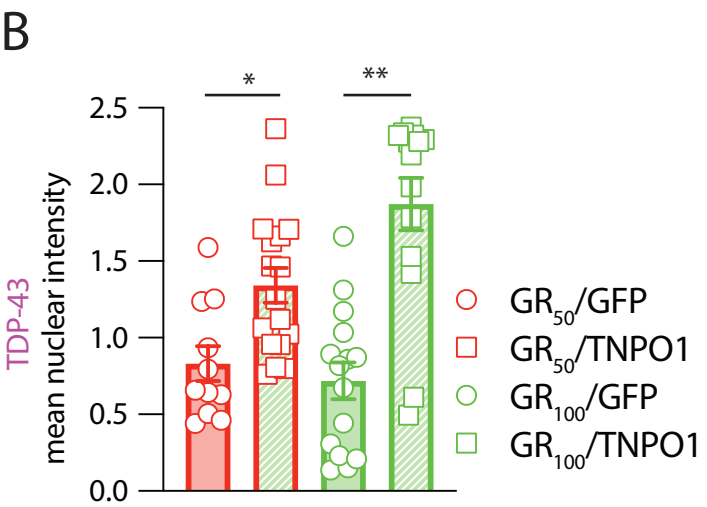

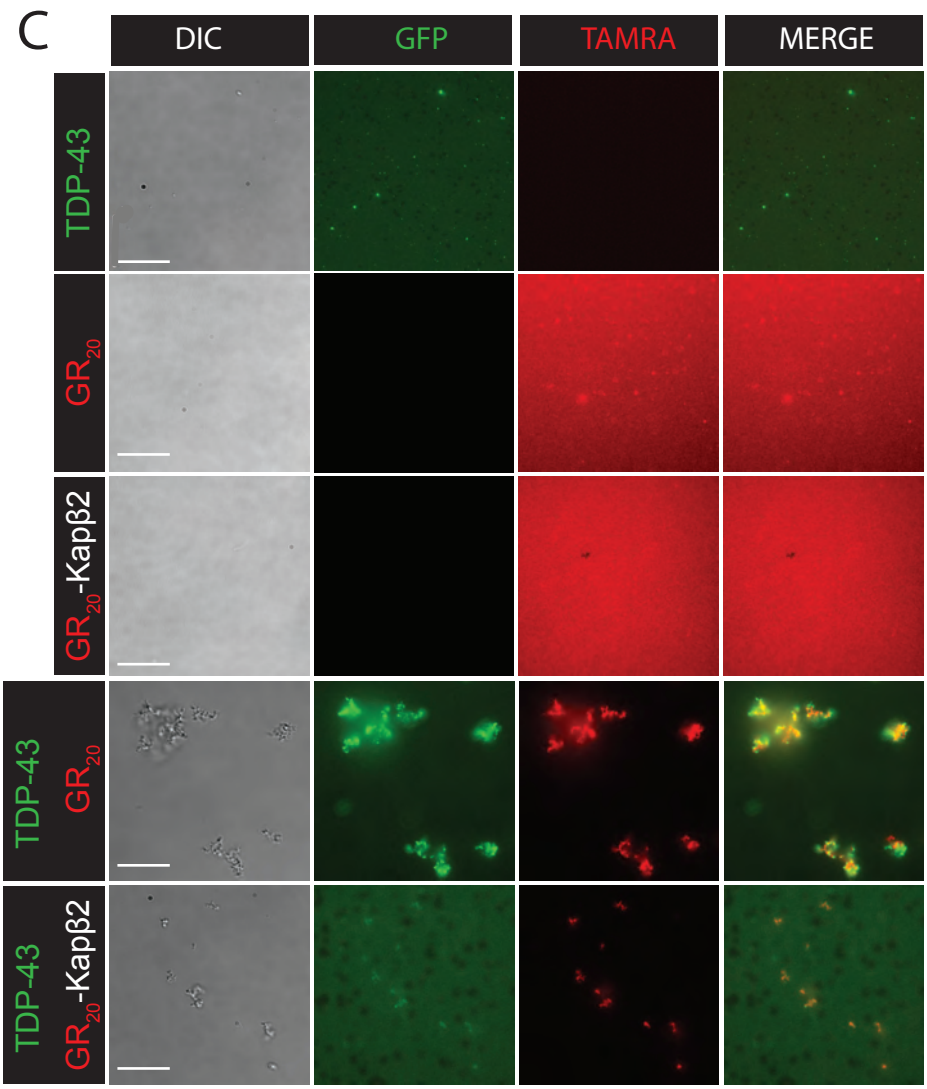

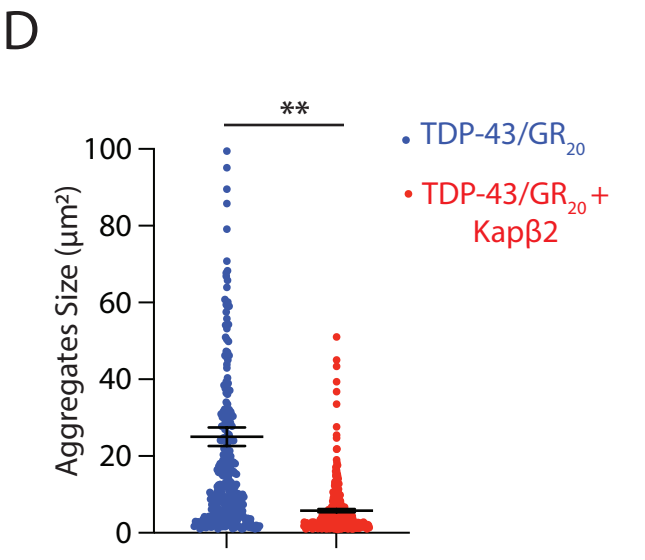

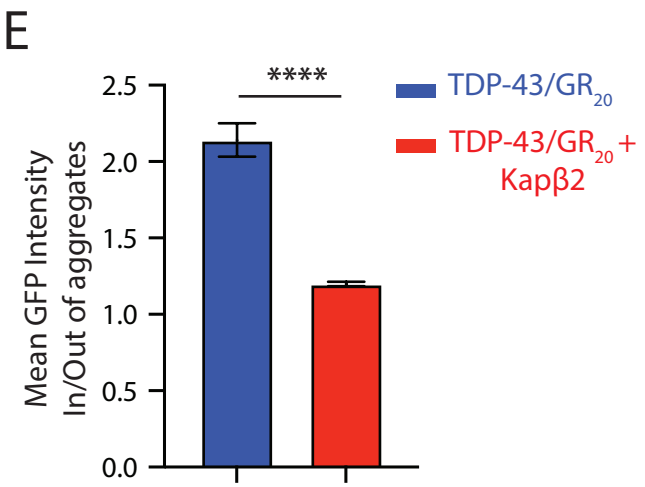

	# cells	p-value	Hazard ratio	95% CI
GFP - 400 ng	447	Reference Group		
GFP-TNPO1 - 400 ng	493	0.0714	1.18	0.9857 to 1.413
GFP - 800 ng	151	Reference Group		
GFP-TNPO1 - 800 ng	264	0.3556	1.13	0.8390 to 1.476

Table 1

	# cells	p-value	Hazard ratio	95% CI
mCherry	811	<0.0001	0.6796	0.5882 to 0.7853
mCherry GR50	722	Reference Group		
mCherry GR50/TNPO1	520	<0.0001	0.6494	0.5538 to 0.7615

	# cells	p-value	Hazard ratio	95% CI
mCherry	811	<0.0001	0.726	0.6242 to 0.8444
mCherry GR100	623	Reference Group		
mCherry GR100/TNPO1	404	0.0054	0.7791	0.6536 to 0.9287

Table 2

Patient	R/G	Year of Death	Age at death
5452	BM		67
5613	WM		70
5572	BF		70
2	WF	2018	63
11	WM	2019	58
29	WM	2019	58

R/G = Race/Gender
M=Male
F=Female
W=White
B=Black

Table 3

Diagnosis	C9ORF72	control	Autopsy Source
None	N\A	Yes	NIH neuro bio bank
None	N\A	Yes	NIH neuro bio bank
None	N\A	Yes	NIH neuro biobank
fALS	YES		JWAC bio bank
fALS	YES		JWAC bio bank
fALS	YES		JWAC bio bank

Table 3